Journal of Theoretical and Applied Mechanics, Sofia, Vol. 47 No. 3 (2017) pp. 25-58

FLUID MECHANICS

HEAT AND MASS TRANSFER OF UNSTEADY HYDROMAGNETIC FREE CONVECTION FLOW THROUGH POROUS MEDIUM PAST A VERTICAL PLATE WITH UNIFORM SURFACE HEAT FLUX

MOHAMED ABD EL-AZIZ[1,2*], AISHAH S. YAHYA[1]

[1]*King Khalid University, Faculty of Science, Mathematics Department, Abha 9004, Saudi Arabia*

[2]*Helwan University,Faculty of Science, Mathematics Department, P.O.Box, 11795, Cairo, Egypt*

[Received 14 October 2016. Accepted 26 June 2017]

ABSTRACT: Simultaneous effects of thermal and concentration diffusions in unsteady magnetohydrodynamic free convection flow past a moving plate maintained at constant heat flux and embedded in a viscous fluid saturated porous medium is presented. The transport model employed includes the effects of thermal radiation, heat sink, Soret and chemical reaction. The fluid is considered as a gray absorbing-emitting but non-scattering medium and the Rosseland approximation in the energy equations is used to describe the radiative heat flux for optically thick fluid. The dimensionless coupled linear partial differential equations are solved by using Laplace transform technique. Numerical results for the velocity, temperature, concentration as well as the skin friction coefficient and the rates of heat and mass transfer are shown graphically for different values of physical parameters involved.

KEY WORDS: Magnetic field; free convection; porous medium; heat flux; heat absorption; chemical reaction.

1. INTRODUCTION

Process involving coupled heat and mass transfer occurs frequently in nature. It occurs not only due to the temperature differences, but also, due to concentration differences or the combination of the two in different geophysical cases. Free convection flow of magnetohydrodynamic fluid has attracted many researchers in view of its numerous applications in geophysics, astrophysics, meteorology, aerodynamics, magnetohydrodynamic power generators and pumps, boundary layer control energy generators, accelerators, aerodynamics heating, polymer technology, petroleum industry, purification of crude oil, and in material processing such as extrusion, metal forming, continuous casting wire, and glass fiber drawing. Muthucumaraswamy *et*

*Corresponding author e-mail: m_abdelaziz999@yahoo.com

al. [1] investigated the flow past an impulsively started infinite vertical plate in the presence of uniform heat and mass flux at the plate and presented an exact solution using Laplace transform technique. Chaudhary and Jain [2] have also studied combined heat and mass transfer effects on MHD free convection flow past an oscillating plate, whereas Sivaiah *et al*. [3] and Das and Jana [4] have studied heat and mass transfer effects on MHD free convection flow past a vertical plate with different boundary conditions.

Further, convection in porous media has gained significant attention in recent years because of its importance in engineering applications such as geothermal systems, solid matrix heat exchangers, thermal insulations, oil extraction and store of nuclear waste materials. Convection in porous media can also be applied to underground coal gasification, ground water hydrology, iron blast furnaces, wall cooled catalytic reactors, solar power collectors, energy efficient drying processes, cooling of nuclear fuel in shipping flasks, cooling of electronic equipment and natural convection in earth's crust. Many studies, with applications, are gathered in a comprehensive review of convective heat transfer mechanisms through porous media in the book by Nield and Bejan [5]. Also, several researchers considered hydromagnetic natural convection flow past a porous plate considering different aspects of the problem. Mention may be made of the research studies of Chamkha [6, 7], Kim [8], Rahman and Sattar [9], Hayat and Abbas [10] and Rajesh and Varma [11]. In view of such applications, Sattar [12] has discussed the free convection and mass transfer flow through a porous medium past an infinite vertical porous plate with time-dependent temperature and concentration. Rees and Pop [13] investigated the effects of transverse surface waves on the free convective boundary layer induced by a uniform heat flux vertical surface embedded in a porous medium. The magnetic effects on the free convection and mass transfer flow through porous medium were studied by Acharya *et al*. [14], whereas Cheng [15] had presented the phenomenon of natural convection heat and mass transfer near a vertical wavy surface with constant wall temperature and concentration in a porous medium. Toki [16] developed the analytical solutions for free convection and mass transfer flow near a moving vertical porous plate. Recently, Rajesh and Varma [17] observed the heat source effects on MHD flow through a porous medium. Chaudhary and Jain [18] analyzed the magnetohydrodynamic free convection flow past an accelerated surface embedded in a porous medium and obtained the exact solutions for the velocity, temperature, and concentration fields using Laplace transform method. The closed form solutions for the unsteady MHD free convection flow with thermal radiation and mass transfer over a moving vertical plate were developed by Das [19], while Pal and Talukdar [20] have studied the problem of unsteady mixed convection with thermal radiation and first-order chemical reaction on magnetohydrodynamics boundary layer flow of viscous, electrically conducting

fluid past a vertical permeable plate. Seth *et al*. [21] investigated the unsteady MHD free convection flow with radiative heat transfer past an impulsively moving plate with ramped wall temperature. The effects of Hall current and mass transfer on the unsteady MHD free convection flow in a porous channel were analyzed by Khan *et al*. [22].

The study of convective flow with heat and mass transfer under the influence of chemical reaction has practical applications in many areas of science and engineering. This phenomenon plays an important role in the chemical industry, petroleum industry, cooling of nuclear reactors, and packed-bed catalytic reactors so that it has received a considerable amount of attention in recent years. Also, the study of chemical reaction with heat transfer in a porous medium has important engineering applications such as tubular reactors, oxidation of solid materials and synthesis of ceramic materials. intensive studies have been carried out to investigate effects of chemical reaction on different flow and fluid types. The effects of chemical reaction and variable viscosity on hydromagnetic mixed convection heat and mass transfer for Hiemenz flow through porous media with radiation were studied by Seddeek *et al*. [23]. Mahdy [24] investigated the effect of chemical reaction and heat generation or absorption on double-diffusive convection from a vertical truncated cone in a porous media with variable viscosity, whereas Alharbi *et al*. [25] presented the convective heat and mass transfer of an incompressible MHD visco-elastic fluid flow immersed in a porous medium over a stretching sheet with chemical reaction and thermal stratification effects. Shateyi and Motsa [26] studied the problem of unsteady MHD convective heat and mass transfer past an Infinite Vertical Plate in a porous medium with thermal radiation in presence of heat generation/absorption and chemical reaction. The combined effects of Soret and Dufour on an unsteady mixed convection magnetohydrodynamics heat and mass transfer in a micropolar fluid saturated Darcian porous medium in the presence of thermal radiation, heat generation, Ohmic heating and chemical reaction have been investigated by Kasim *et al*. [27]. Ali *et al*. [28] developed the combined effects of heat and mass transfer on free convection unsteady MHD flow of viscous fluid embedded in a porous medium.

The objective of this work is to extend the study of Ali *et al*. [28] to a vertical plate with a uniform surface heat flux immersed in an absorbing fluid, that is, to study the problem of free convection MHD flow of an incompressible, viscous, absorbing fluid past an accelerated vertical plate with constant surface heat flux embedded in a porous medium. The magnetic field is applied normal to the surface of the plate which is electrically insulated. Analytical solutions are developed and the effects of the pertinent parameters on the fluid flow, heat and mass transfer characteristics are discussed in detail through graphs. To the best of authors' knowledge, this problem has not been studied before in literature and the reported results are new.

2. ANALYSIS

Consider the unsteady one-dimensional flow of an incompressible, electrically conducting and viscous fluid past an infinite vertical plate embedded in a porous medium with constant heat flux at $y^* = 0$. The x^*-axis is measured along the plate in the upward direction and y^*-axis is measured normal to the plate in the outward direction. A uniform magnetic field B_0 is acting in the transverse direction to the flow. The transversely applied magnetic field and magnetic Reynolds number are assumed to be very small so that the induced magnetic field and the Hall effect are negligible. The Soret and thermal buoyancy effects are also considered. The plate is infinite in length, so all the field quantities become functions of space coordinate y^* and time t^*. Initially, the plate and the fluid are at same temperature T^*_∞ and concentration C^*_∞. Subsequently, at time $t^* > 0$, the plate begins to move in its own plane and accelerates against the gravitational field with uniform acceleration $f(t^*)$ in x^*-direction. Simultaneously, heat is supplied from the surface of the plate to the fluid, which is maintained throughout the fluid flow at the uniform rate (q''_w/k) and concentration level is raised to C^*_w as shown in Fig. 1. Under the above assumptions and invoking the Boussinesq approximation, the governing equations of momentum, energy and concentration are derived as follows:

$$\frac{\partial u^*}{\partial t^*} = \nu \frac{\partial^2 u*}{\partial y^{*2}} - \frac{\sigma B_0^2}{\rho} u^* - \frac{\nu}{K^*} u^* + g\beta(T^* - T^*_\infty) + g\beta^*(C^* - C^*_\infty), \tag{1}$$

$$\rho c_p \frac{\partial T^*}{\partial t^*} = k \frac{\partial^2 T^*}{\partial y^{*2}} - \frac{\partial q^*_r}{\partial y^*} - Q_0(T^* - T^*_\infty), \tag{2}$$

$$\frac{\partial C^*}{\partial t^*} = D \frac{\partial^2 C^*}{\partial y^{*2}} + \frac{DK_T}{T_m} \frac{\partial^2 T^*}{\partial y^{*2}} - K^*_r(C^* - C^*_\infty), \tag{3}$$

with the following initial and boundary conditions:

$$\begin{aligned}
&t^* \le 0 \ : \quad u^* = 0, && T^* = T^*_\infty, && C^* = C^*_\infty, && \forall\ y^* \ge 0, \\
&t^* > 0 \ : \quad u^* = f(t^*), && \frac{\partial T^*}{\partial y^*} = -\frac{q''_w}{k}, && C^* = C^*_w && \text{at } y^* = 0, \\
&\qquad\quad : \quad u^* \longrightarrow 0, && T^* \longrightarrow T^*_\infty, && C^* \longrightarrow C^*_\infty && \text{as } y^* \longrightarrow \infty,
\end{aligned} \tag{4}$$

in which $f(t^*)$ is the uniform acceleration of the plate, x^* and y^* are the distances along and perpendicular to the plate, t^* is the dimensional time, u^* is the fluid velocity in the x^*-direction, T^* is the temperature of the fluid, T^*_∞ is the free stream temperature, C^* is the concentration, C^*_w is the surface concentration, C^*_∞ is the free stream concentration, Q_0 is the dimensional heat absorption coefficient, k is the thermal conductivity, q^*_r is the radiative heat flux in x^*-direction, q''_w is the constant heat

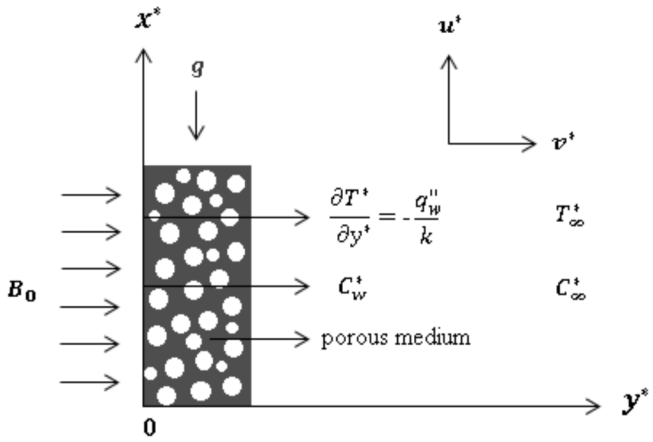

Fig. 1. Flow geometry and physical coordinate system.

flux per unit area at the plate, β is the volumetric coefficient of thermal expansion, β^* is the volumetric coefficient of expansion for concentration, ν is the kinematic viscosity, μ is the fluid viscosity, ρ is the fluid density, c_p is the specific heat capacity, σ is the electrical conductivity of the fluid, K^* is the permeability of the porous medium, T_m is the mean fluid temperature, K_T is the thermal-diffusion ratio, K_r^* is the chemical reaction constant and D is the mass diffusivity.

The radiative heat flux q_r^* under Rosseland approximation has the form

$$q_r^* = \frac{-4\sigma^*}{3k^*}\frac{\partial T^{*4}}{\partial y^*}, \tag{5}$$

where σ^* is the Stefan-Boltzmann constant and k^* is the mean absorption coefficient. It is assumed that the temperature differences within the flow are sufficiently small such that the term T^{*4} is expressed as the linear function of temperature. Thus expanding T^{*4} about T_∞^* using Taylor series expansion and neglecting higher order terms

$$T^{*4} \simeq T_\infty^{*4} + 4T_\infty^{*3}(T^* - T_\infty^*) \simeq 4T_\infty^{*3}T^* - 3T_\infty^{*4}$$

gives

$$q_r^* = \frac{-16\sigma^* T_\infty^{*3}}{3k^*}\frac{\partial T^*}{\partial y^*}. \tag{6}$$

From (6), (2) reduces to the following form:

$$\rho c_p \frac{\partial T^*}{\partial t^*} = k\frac{\partial^2 T^*}{\partial y^{*2}} + \frac{16\sigma^* T_\infty^{*3}}{3k^*}\frac{\partial^2 T^*}{\partial y^{*2}} - Q_0(T^* - T_\infty^*). \tag{7}$$

Now, we take $f(t^*) = At^*$ and define the following non-dimensional variables:

$$\theta = \frac{T^* - T^*_\infty}{\left(\frac{q''_w}{k}\right)\sqrt[3]{\frac{\nu^2}{A}}}, \qquad \phi = \frac{C^* - C^*_\infty}{C^*_w - C^*_\infty}, \qquad u = \frac{u^*}{\sqrt[3]{\nu A}},$$
$$y = y^*\sqrt[3]{\frac{A}{\nu^2}}, \qquad t = t^*\sqrt[3]{\frac{A^2}{\nu}}, \tag{8}$$

where A denotes the uniform acceleration of the plate in x-direction, u is the dimensionless velocity, y dimensionless coordinate perpendicular to the plate, t is the dimensionless time, θ is the dimensionless temperature and ϕ is the dimensionless species concentration. Substituting Eqs. (8) into Eqs. (1), (3) and (7) gives the governing equations in dimensionless form

$$\frac{\partial u}{\partial t} = \frac{\partial^2 u}{\partial y^2} - Hu + Gr\theta + Gm\phi, \tag{9}$$

$$F^*\frac{\partial \theta}{\partial t} = \frac{\partial^2 \theta}{\partial y^2} - L\theta, \tag{10}$$

$$\frac{\partial \phi}{\partial t} = \frac{1}{Sc}\frac{\partial^2 \phi}{\partial y^2} + Sr\frac{\partial^2 \theta}{\partial y^2} - \gamma\phi, \tag{11}$$

with dimensionless initial and boundary conditions

$$\begin{aligned} t \le 0 \ : \quad & u = 0, \quad \theta = 0, \qquad \phi = 0, \ y \ge 0, \\ t > 0 \ : \quad & u = t, \quad \frac{\partial \theta}{\partial y} = -1, \quad \phi = 1 \text{ at } y = 0, \\ : \quad & u \to 0, \quad \theta \to 0, \qquad \phi \to 0 \text{ as } y \to \infty, \end{aligned} \tag{12}$$

where

$$\begin{aligned} M &= \frac{\sigma B_0^2 \sqrt[3]{\nu A}}{\rho A}, \quad Gr = \frac{g\beta q''_w \sqrt[3]{\frac{\nu^2}{A}}}{kA}, \quad Gm = \frac{g\beta^*(C^*_w - C^*_\infty)}{A}, \\ \frac{1}{K} &= \frac{\nu\sqrt[3]{\nu A}}{AK^*}, \quad H = M + \frac{1}{K}, \quad Pr = \frac{\nu\rho c_p}{k}, \quad R = \frac{16\sigma^* T^{*3}_\infty}{3kk^*}, \\ Q_H &= \frac{Q_0}{\rho c_p \sqrt[3]{\frac{A^2}{\nu}}}, \quad F^* = \frac{Pr}{1+R}, \quad L = F^* Q_H, \quad Sc = \frac{\nu}{D}, \\ Sr &= \frac{DK_T q''_w \sqrt[3]{\frac{1}{\nu A}}}{(C^*_w - C^*_\infty)T_m k}, \quad \gamma = K^*_r \sqrt[3]{\frac{\nu}{A^2}}. \end{aligned} \tag{13}$$

Here, M is the magnetic parameter, K is the dimensionless permeability, Sc is Schmidt number, R is radiation parameter, Gr is Grashof number for heat transfer , Gm is Grashof number for mass transfer, Q_H is the heat absorption parameter, Sr is Soret number and γ is the chemical reaction parameter. It should be mentioned here that $\gamma > 0$ indicates a destructive chemical reaction while $\gamma < 0$ corresponds to a generative chemical reaction. The well-posed problems defined by (9) – (11) will be solved by using the Laplace transform technique. Exact analytical expressions for dimensionless temperature, concentration and velocity fields will be separately obtained for $Sc \neq 1$ and $Sc = 1$.

2.1. THE CASE SC $\neq 1$

By employing Laplace transform technique, we can obtain the solution of equations (9), (10) and (11) subject to conditions (12). Therefore, the problem in the transformed plane is given as

$$\frac{d^2\overline{u}}{dy^2} - (H+s)\overline{u} + Gr\overline{\theta} + Gm\overline{\phi} = 0, \tag{14}$$

$$\frac{d^2\overline{\theta}}{dy^2} - (L + F^* s)\overline{\theta} = 0, \tag{15}$$

$$\frac{d^2\overline{\phi}}{dy^2} + Sr\, Sc \frac{d^2\overline{\theta}}{dy^2} - (s+\gamma)\, Sc\, \overline{\phi} = 0, \tag{16}$$

with the corresponding transformed boundary conditions

$$\begin{aligned} &\overline{u}(0,s) = \frac{1}{s^2}, && \overline{u}(\infty,s) = 0, \\ &\frac{d\overline{\theta}(0,s)}{dy} = -\frac{1}{s}, && \overline{\theta}(\infty,s) = 0, \\ &\overline{\phi}(0,s) = \frac{1}{s}, && \overline{\phi}(\infty,s) = 0, \end{aligned} \tag{17}$$

where s is the Laplace transformation parameter. The solutions of (14),(15) and (16) in the transformed s-plane are given by

$$\begin{aligned} \overline{u}(y,s) = {} & \frac{\exp\left(-y\sqrt{H+s}\right)}{s^2} - \frac{a_1\sqrt{s+Q_H}\exp\left(-y\sqrt{H+s}\right)}{s(s-H^*)(s-H_1^*)} \\ & + \frac{Gr^*\exp\left(-y\sqrt{H+s}\right)}{s(s-H^*)\sqrt{F^*(s+Q_H)}} + \frac{a_2\exp\left(-y\sqrt{H+s}\right)}{s(s+a_0)} \\ & + \frac{a_3\sqrt{s+Q_H}\exp\left(-y\sqrt{H+s}\right)}{s(s+a_0)(s-H_1^*)} - \frac{Gr^*\exp\left(-y\sqrt{F^*(s+Q_H)}\right)}{s(s-H^*)\sqrt{F^*(s+Q_H)}} \end{aligned} \tag{18}$$

$$+\frac{a_1\sqrt{s+Q_H}\exp\big(-y\sqrt{F^*(s+Q_H)}\big)}{s(s-H^*)(s-H_1^*)}-\frac{a_2\exp\big(-y\sqrt{Sc(\gamma+s)}\big)}{s(s+a_0)}$$
$$-\frac{a_3\sqrt{s+Q_H}\exp\big(-y\sqrt{Sc(\gamma+s)}\big)}{s(s+a_0)(s-H_1^*)},$$

$$\overline{\theta}(y,s)=\frac{\exp\Big(-y\sqrt{F^*(s+Q_H)}\Big)}{s\sqrt{F^*(s+Q_H)}}, \tag{19}$$

$$\overline{\phi}(y,s)=\frac{\exp\Big(-y\sqrt{Sc(s+\gamma)}\Big)}{s}+\frac{S^*\sqrt{s+Q_H}\ \exp\Big(-y\sqrt{Sc(s+\gamma)}\Big)}{s(s-H_1^*)}$$
$$-\frac{S^*\sqrt{s+Q_H}\ \exp\Big(-y\sqrt{F^*(s+Q_H)}\Big)}{s(s-H_1^*)}, \tag{20}$$

where

$$\begin{aligned}
&a_0=\frac{Sc\,\gamma-H}{Sc-1}, && a_1=\frac{S^*Gm}{F^*-1}, && a_2=\frac{Gm}{Sc-1},\\
&a_3=\frac{GmS^*}{Sc-1}, && S^*=\frac{SrSc\sqrt{F^*}}{F^*-Sc}, && Gr^*=\frac{Gr}{F^*-1},\\
&H^*=\frac{H-F^*Q_H}{F^*-1}, && H_1^*=\frac{Sc\gamma-F^*Q_H}{F^*-Sc}.
\end{aligned} \tag{21}$$

The inverse Laplace transform of (18), (19) and (20) yields

$$u(y,t)=I_1-I_2+I_3+I_4+I_5-I_6+I_7-I_8-I_9, \tag{22}$$

$$\theta(y,t)=\frac{1}{2\sqrt{F^*\,Q_H}}\Bigg[\exp(-y\sqrt{F^*\,Q_H})\,\mathrm{erfc}\Big(\frac{y\sqrt{F^*}}{2\sqrt{t}}-\sqrt{Q_Ht}\Big)$$
$$-\exp\big(y\sqrt{F^*\,Q_H}\big)\,\mathrm{erfc}\Big(\frac{y\sqrt{F^*}}{2\sqrt{t}}+\sqrt{Q_Ht}\Big)\Bigg], \tag{23}$$

$$\phi(y,t)=J_1+J_2-J_3, \tag{24}$$

where $\mathrm{erf}(x)$ is the error function and $\mathrm{erfc}(x)$ is the complementary error function with

$$I_1 = \frac{1}{2}\Bigg[\Big(t - \frac{y}{2\sqrt{H}}\Big)\exp\big(-y\sqrt{H}\big)\mathrm{erfc}\Big(\frac{y}{2\sqrt{t}} - \sqrt{H\,t}\Big) + \Big(t + \frac{y}{2\sqrt{H}}\Big)\exp\Big(y\sqrt{H}\Big)\mathrm{erfc}\Big(\frac{y}{2\sqrt{t}} + \sqrt{H\,t}\Big)\Bigg],$$

$$I_2 = \frac{a_1}{2}\int_0^t \Bigg[\frac{\sqrt{H^* + Q_H}}{H^*}\exp(H^*(t-u))\mathrm{erf}\Big(\sqrt{(t-u)(H^*+Q_H)}\Big) - \frac{\sqrt{Q_H}}{H^*}\,\mathrm{erf}\Big(\sqrt{Q_H(t-u)}\Big)\Bigg]\exp(H_1^* u)\Bigg[\exp(-y\sqrt{H_1^*+H}) \times \mathrm{erfc}\Big(\frac{y}{2\sqrt{u}} - \sqrt{u(H_1^*+H)}\Big) + \exp\big(y\sqrt{H_1^*+H}\big) \times \mathrm{erfc}\Big(\frac{y}{2\sqrt{u}} + \sqrt{u(H_1^*+H)}\Big)\Bigg]du,$$

$$I_3 = \frac{Gr^*}{2}\int_0^t \frac{\mathrm{erf}\Big(\sqrt{Q_H(t-u)}\Big)}{\sqrt{F^* Q_H}}\exp\left(H^* u\right) \times \Bigg[\exp\Big(-y\sqrt{H^*+H}\Big)\,\mathrm{erfc}\Big(\frac{y}{2\sqrt{u}} - \sqrt{u(H^*+H)}\Big) + \exp\Big(y\sqrt{H^*+H}\Big)\,\mathrm{erfc}\Big(\frac{y}{2\sqrt{u}} + \sqrt{u(H^*+H)}\Big)\Bigg]du,$$

$$I_4 = \frac{a_2}{2}\int_0^t \exp(-a_0 u)\Bigg[\exp(-y\sqrt{H-a_0})\mathrm{erfc}\Big(\frac{y}{2\sqrt{u}} - \sqrt{u(H-a_0)}\Big) + \exp(y\sqrt{H-a_0})\mathrm{erfc}\Big(\frac{y}{2\sqrt{u}} + \sqrt{u(H-a_0)}\Big)\Bigg]du,$$

$$I_5 = \frac{a_3}{2}\int_0^t \Big[\frac{\sqrt{H_1^*+Q_H}}{H_1^*}\exp(H_1^*(t-u))\mathrm{erf}\Big(\sqrt{(t-u)(H_1^*+Q_H)}\Big) - \frac{\sqrt{Q_H}}{H_1^*}\mathrm{erf}\left(\sqrt{Q_H(t-u)}\right)\Big] \times \exp(-a_0u)\Bigg[\exp\left(-y\sqrt{H-a_0}\right)\mathrm{erfc}\Big(\frac{y}{2\sqrt{u}}-\sqrt{u(H-a_0)}\Big) + \exp\left(y\sqrt{H-a_0}\right)\mathrm{erfc}\Big(\frac{y}{2\sqrt{u}}+\sqrt{u(H-a_0)}\Big)\Bigg]du,$$

$$I_6 = \frac{Gr^*}{2}\int_0^t \Big[\frac{\mathrm{erf}\left(\sqrt{Q_H(t-u)}\right)}{\sqrt{F^*Q_H}}\Big]\exp(H^*u) \times \Bigg[\exp\left(-y\sqrt{F^*(H^*+Q_H)}\right)\mathrm{erfc}\Big(\frac{y\sqrt{F^*}}{2\sqrt{u}}-\sqrt{u(H^*+Q_H)}\Big) + \exp\left(y\sqrt{F^*(H^*+Q_H)}\right)\mathrm{erfc}\Big(\frac{y\sqrt{F^*}}{2\sqrt{u}}+\sqrt{u(H^*+Q_H)}\Big)\Bigg]du,$$

$$I_7 = \frac{a_1}{2}\int_0^t \Big[\frac{\sqrt{H_1^*+Q_H}}{H_1^*}\exp(H_1^*(t-u))\mathrm{erf}\left(\sqrt{(t-u)(H_1^*+Q_H)}\right) - \frac{\sqrt{Q_H}}{H_1^*}\mathrm{erf}\left(\sqrt{Q_H(t-u)}\right)\Big]\exp(H^*u) \times \Bigg[\exp\left(-y\sqrt{F^*(H^*+Q_H)}\right)\mathrm{erfc}\Big(\frac{y\sqrt{F^*}}{2\sqrt{u}}-\sqrt{u(H^*+Q_H)}\Big) + \exp\left(y\sqrt{F^*(H^*+Q_H)}\right)\mathrm{erfc}\Big(\frac{y\sqrt{F^*}}{2\sqrt{u}}+\sqrt{u(H^*+Q_H)}\Big)\Bigg]du,$$

$$I_8 = \frac{a_2}{2}\int_0^t \exp(-a_0u)\Bigg[\exp\left(-y\sqrt{Sc(\gamma-a_0)}\right)\mathrm{erfc}\Big(\frac{y\sqrt{Sc}}{2\sqrt{u}}-\sqrt{u(\gamma-a_0)}\Big) + \exp\left(y\sqrt{Sc(\gamma-a_0)}\right)\mathrm{erfc}\Big(\frac{y\sqrt{Sc}}{2\sqrt{u}}+\sqrt{u(\gamma-a_0)}\Big)\Bigg]du,$$

$$I_9 = \frac{a_3}{2}\int_0^t \Big[\frac{\sqrt{H_1^*+Q_H}}{H_1^*}\exp(H_1^*(t-u))\text{erf}\left(\sqrt{(t-u)(H_1^*+Q_H)}\right) - \frac{\sqrt{Q_H}}{H_1^*}\text{erf}\left(\sqrt{Q_H(t-u)}\right)\Big]\exp(-a_0u) \times \left[\exp\left(-y\sqrt{Sc(\gamma-a_0)}\right)\text{erfc}\Big(\frac{y\sqrt{Sc}}{2\sqrt{u}} - \sqrt{u(\gamma-a_0)}\Big) + \exp\left(y\sqrt{Sc(\gamma-a_0)}\right)\text{erfc}\Big(\frac{y\sqrt{Sc}}{2\sqrt{u}} + \sqrt{u(\gamma-a_0)}\Big)\right]du,$$

$$J_1 = \frac{1}{2}\left[\exp(-y\sqrt{Sc\gamma})\text{erfc}\Big(\frac{y\sqrt{Sc}}{2\sqrt{t}} - \sqrt{\gamma t}\Big) + \exp(y\sqrt{Sc\,\gamma})\text{erfc}\Big(\frac{y\sqrt{Sc}}{2\sqrt{t}} + \sqrt{\gamma t}\Big)\right],$$

$$J_2 = \frac{S^*}{2}\int_0^t \Big[\sqrt{Q_H}\,\text{erf}\left(\sqrt{Q_H\,(t-u)}\right) + \frac{\exp(-Q_H(t-u))}{\sqrt{\pi(t-u)}}\Big]\exp\left(H_1^*u\right) \times \left[\exp\left(-y\sqrt{Sc(\gamma+H_1^*)}\right)\text{erfc}\Big(\frac{y\sqrt{Sc}}{2\sqrt{u}} - \sqrt{u(\gamma+H_1^*)}\Big) + \exp\left(y\sqrt{Sc(\gamma+H_1^*)}\right)\text{erfc}\Big(\frac{y\sqrt{Sc}}{2\sqrt{u}} + \sqrt{u(\gamma+H_1^*)}\Big)\right]du,$$

$$J_3 = \frac{S^*}{2}\int_0^t \Big[\sqrt{Q_H}\,\text{erf}\left(\sqrt{Q_H\,(t-u)}\right) + \frac{\exp\left(-Q_H(t-u)\right)}{\sqrt{\pi(t-u)}}\Big]\exp\left(H_1^*u\right) \times \left[\exp\left(-y\sqrt{F^*(H_1^*+Q_H)}\right)\text{erfc}\Big(\frac{y\sqrt{F^*}}{2\sqrt{u}} - \sqrt{u(H_1^*+Q_H)}\Big) + \exp\left(y\sqrt{F^*(H_1^*+Q_H)}\right)\text{erfc}\Big(\frac{y\sqrt{F^*}}{2\sqrt{u}} + \sqrt{u(H_1^*+Q_H)}\Big)\right]du.$$

2.2. THE CASE SC = 1

In this case, the solutions of (14), (15) and (16) subject to the boundary conditions (17) are given by

$$u(y,t) = I_1 - I_{10} + I_3 + I_{11} + I_{12} - I_6 + I_{13} - I_{14} - I_{15}, \tag{25}$$

$$\theta(y,t) = \frac{1}{2\sqrt{F^*\,Q_H}}\Bigg[\exp\Big(-y\sqrt{F^*\,Q_H}\Big)\,\mathrm{erfc}\Big(\frac{y\sqrt{F^*}}{2\sqrt{t}} - \sqrt{Q_H t}\Big) - \exp\Big(y\sqrt{F^*\,Q_H}\Big)\,\mathrm{erfc}\Big(\frac{y\sqrt{F^*}}{2\sqrt{t}} + \sqrt{Q_H t}\Big)\Bigg], \tag{26$\equiv$ 23}$$

$$\phi(y,t) = J_4 + J_5 - J_6, \tag{27}$$

where

$$I_{10} = \frac{a_4}{2}\int_0^t \Bigg[\frac{\sqrt{H^*+Q_H}}{H^*}\exp\left(H^*(t-u)\right)\mathrm{erf}\Big(\sqrt{(t-u)(H^*+Q_H)}\Big) - \frac{\sqrt{Q_H}}{H^*}\mathrm{erf}\Big(\sqrt{Q_H(t-u)}\Big)\Bigg]\exp(H_2^*u)\Bigg[\exp\Big(-y\sqrt{H_2^*+H}\Big) \times \mathrm{erfc}\Big(\frac{y}{2\sqrt{u}} - \sqrt{u(H_2^*+H)}\Big) + \exp\Big(y\sqrt{H_2^*+H}\Big) \times \mathrm{erfc}\Big(\frac{y}{2\sqrt{u}} + \sqrt{u(H_2^*+H)}\Big)\Bigg]du,$$

$$I_{11} = \frac{a_5}{2}\Big[\exp\Big(-y\sqrt{H}\Big)\,\mathrm{erfc}\Big(\frac{y}{2\sqrt{t}} - \sqrt{H\,t}\Big) + \exp\Big(y\sqrt{H}\Big)\,\mathrm{erfc}\Big(\frac{y}{2\sqrt{t}} + \sqrt{Ht}\Big)\Big],$$

$$I_{12} = \frac{a_6}{2}\int_0^t \Bigg[\frac{\exp\left(-Q_H(t-u)\right)}{\sqrt{\pi(t-u)}} + \exp(H_2^*(t-u)) \times \mathrm{erf}\Big(\sqrt{(t-u)(Q_H+H_2^*)}\Big)\sqrt{Q_H+H_2^*}\Bigg]\Bigg[\exp\Big(-y\sqrt{H}\Big) \times \mathrm{erfc}\Big(\frac{y}{2\sqrt{u}} - \sqrt{H\,u}\Big) + \exp\Big(y\sqrt{H}\Big)\,\mathrm{erfc}\Big(\frac{y}{2\sqrt{u}} + \sqrt{Hu}\Big)\Bigg]du,$$

$$I_{13} = \frac{a_4}{2}\int_0^t \left[\frac{\sqrt{H^*+Q_H}}{H^*}\exp(H^*(t-u))\text{erf}\left(\sqrt{(t-u)(H^*+Q_H)}\right) - \frac{\sqrt{Q_H}}{H^*}erf\left(\sqrt{Q_H(t-u)}\right)\right]\exp(H_2^*u)$$
$$\times\left[\exp\left(-y\sqrt{F^*(H_2^*+Q_H)}\right)\text{erfc}\left(\frac{y\sqrt{F^*}}{2\sqrt{u}} - \sqrt{u(H_2^*+Q_H)}\right) + \exp\left(y\sqrt{F^*(H_2^*+Q_H)}\right)\text{erfc}\left(\frac{y\sqrt{F^*}}{2\sqrt{u}} + \sqrt{u(H_2^*+Q_H)}\right)\right]du,$$

$$I_{14} = \frac{a_5}{2}\Big[\exp(-y\sqrt{\gamma})\text{erfc}\Big(\frac{y}{2\sqrt{t}} - \sqrt{\gamma t}\Big) + \exp(y\sqrt{\gamma})\text{erfc}\Big(\frac{y}{2\sqrt{t}} + \sqrt{\gamma t}\Big)\Big],$$

$$I_{15} = \frac{a_6}{2}\int_0^t \left[\frac{\exp\left(-Q_H(t-u)\right)}{\sqrt{\pi(t-u)}} + \exp(H_2^*(t-u))\text{erf}\left(\sqrt{(t-u)(Q_H+H_2^*)}\right)\times\sqrt{Q_H+H_2^*}\right]\left[\exp\left(-y\sqrt{\gamma}\right)\text{erfc}\Big(\frac{y}{2\sqrt{u}} - \sqrt{\gamma u}\Big) + \exp\left(y\sqrt{\gamma}\right)\text{erfc}\Big(\frac{y}{2\sqrt{u}} + \sqrt{\gamma\, u}\Big)\right]du,$$

also

$$J_4 = \frac{1}{2}\Big[\exp(-y\sqrt{\gamma})\text{erfc}\Big(\frac{y}{2\sqrt{t}} - \sqrt{\gamma t}\Big) + \exp(y\sqrt{\gamma})\text{erfc}\Big(\frac{y}{2\sqrt{t}} + \sqrt{\gamma t}\Big)\Big]$$

$$J_5 = \frac{S_1^*}{2}\int_0^t \Big[\sqrt{Q_H}\,\text{erf}(\sqrt{Q_H(t-u)}) + \frac{\exp(-Q_H(t-u))}{\sqrt{\pi(t-u)}}\Big]\times\exp(H_2^*u)\left[\exp(-y\sqrt{\gamma+H_2^*})\text{erfc}\Big(\frac{y}{2\sqrt{u}} - \sqrt{u(\gamma+H_2^*)}\Big) + \exp(y\sqrt{\gamma+H_2^*})\,\text{erfc}\Big(\frac{y}{2\sqrt{u}} + \sqrt{u(\gamma+H_2^*)}\Big)\right]du,$$

$$J_6 = \frac{S_1^*}{2}\int_0^t \Big[\sqrt{Q_H}\,\mathrm{erf}(\sqrt{Q_H\,(t-u)}) + \frac{\exp(-Q_H(t-u))}{\sqrt{\pi(t-u)}}\Big]\exp(H_2^* u)$$
$$\Bigg[\exp(-y\sqrt{F^*(H_2^*+Q_H)})\,\mathrm{erfc}\Big(\frac{y\sqrt{F^*}}{2\sqrt{u}} - \sqrt{u(H_2^*+Q_H)}\Big)$$
$$+ \exp(y\sqrt{F^*(H_2^*+Q_H)})\,\mathrm{erfc}\Big(\frac{y\sqrt{F^*}}{2\sqrt{u}} + \sqrt{u(H_2^*+Q_H)}\Big)\Bigg]du,$$

and

$$S_1^* = \frac{Sr\sqrt{F^*}}{F^*-1}, \qquad H_2^* = \frac{\gamma - F^*\,Q_H}{F^*-1},$$
$$a_4 = \frac{S_1^*\,Gm}{F^*-1}, \qquad a_5 = \frac{Gm}{\gamma - H}, \qquad a_6 = \frac{Gm\,S_1^*}{\gamma - H}.$$

2.3. SKIN FRICTION

The expression of skin friction coefficient is given by

$$\tau = \frac{-\mu}{\rho(A\nu)^{2/3}}\frac{\partial u^*}{\partial y^*}\Big|_{y^*=0} = -\frac{\partial u}{\partial y}\Big|_{y=0} \tag{28}$$
$$= -(\tau_1 - \tau_2 + \tau_3 + \tau_4 + \tau_5 - \tau_6 + \tau_7 - \tau_8 - \tau_9),$$

where

$$\tau_i = \frac{\partial I_i}{\partial\, y}\Big|_{y=0}, \qquad i = 1, 2, ..., 9$$

and

$$\tau_1 = -\frac{1}{2}\left(\frac{2\sqrt{t}\exp(-H\,t)}{\sqrt{\pi}} + \frac{\mathrm{erf}(\sqrt{H\,t})}{\sqrt{H}} + 2t\sqrt{H}\,\mathrm{erf}(\sqrt{H\,t})\right),$$

$$\tau_2 = \frac{a_1}{2}\int_0^t \Bigg[\frac{\sqrt{H^*+Q_H}}{H^*}\exp(H^*(t-u))\mathrm{erf}\left(\sqrt{(t-u)(H^*+Q_H)}\right)$$
$$- \frac{\sqrt{Q_H}}{H^*}\,\mathrm{erf}\left(\sqrt{Q_H(t-u)}\right)\Bigg]\exp(H_1^* u)$$
$$\times\Big[\frac{-2\exp(-u(H_1^*+H))}{\sqrt{\pi u}} - 2\sqrt{H_1^*+H}\;\mathrm{erf}\left(\sqrt{u\,(H_1^*+H)}\right)\Big]du,$$

$$\tau_3 = \frac{Gr^*}{2}\int_0^t \frac{\text{erf}\left(\sqrt{Q_H(t-u)}\right)}{\sqrt{F^*Q_H}}\left[\frac{-2\exp(-u(H^*+H))}{\sqrt{\pi u}} - 2\sqrt{H^*+H}\,\text{erf}\left(\sqrt{u\,(H^*+H)}\right)\right]\exp(H^*u)du,$$

$$\tau_4 = \frac{a_2}{2}\int_0^t \exp(-a_0u)\left[\frac{-2\exp(-u(H-a_0))}{\sqrt{\pi u}} - 2\sqrt{H-a_0}\,\text{erf}\left(\sqrt{u(H-a_0)}\right)\right]du,$$

$$\tau_5 = \frac{a_3}{2}\int_0^t \left[\frac{\sqrt{H_1^*+Q_H}}{H_1^*}\exp(H_1^*(t-u))\text{erf}\left(\sqrt{(t-u)(H_1^*+Q_H)}\right) - \frac{\sqrt{Q_H}}{H_1^*}\,\text{erf}\left(\sqrt{Q_H(t-u)}\right)\right]\exp(-a_0u)\left[\frac{-2\exp(-u\,(H-a_0))}{\sqrt{\pi u}} - 2\sqrt{H-a_0}\,\text{erf}\left(\sqrt{u(H-a_0)}\right)\right]du,$$

$$\tau_6 = \frac{Gr^*}{2}\int_0^t \left[\frac{-2\sqrt{F^*}\,\exp(-u(H^*+Q_H))}{\sqrt{\pi u}} - 2\sqrt{F^*(H^*+Q_H)} \times \text{erf}\left(\sqrt{u(H^*+Q_H)}\right)\right]\exp(H^*u)\left[\frac{\text{erf}\left(\sqrt{Q_H(t-u)}\right)}{\sqrt{F^*Q_H}}\right]du,$$

$$\tau_7 = \frac{a_1}{2}\int_0^t \left[\frac{\sqrt{H_1^*+Q_H}}{H_1^*}\,\exp(H_1^*(t-u))\text{erf}\left(\sqrt{(t-u)(H_1^*+Q_H)}\right) - \frac{\sqrt{Q_H}}{H_1^*}\,\text{erf}\left(\sqrt{Q_H(t-u)}\right)\right]\exp(H^*u)\left[\frac{-2\sqrt{F^*}\,\exp(-u(H^*+Q_H))}{\sqrt{\pi u}} - 2\sqrt{F^*(H^*+Q_H)}\,\text{erf}\left(\sqrt{u(H^*+Q_H)}\right)\right]du,$$

$$\tau_8 = \frac{a_2}{2}\int_0^t \exp(-a_0 u)\left[\frac{-2\sqrt{Sc}\exp(-u(\gamma-a_0))}{\sqrt{\pi u}} - 2\sqrt{Sc(\gamma-a_0)}\ \text{erf}\left(\sqrt{u(\gamma-a_0)}\right)\right]du,$$

$$\tau_9 = \frac{a_3}{2}\int_0^t \left[\frac{\sqrt{H_1^*+Q_H}}{H_1^*}\exp(H_1^*(t-u))\,\text{erf}\left(\sqrt{(t-u)(H_1^*+Q_H)}\right) - \frac{\sqrt{Q_H}}{H_1^*}\,\text{erf}\left(\sqrt{Q_H(t-u)}\right)\right]\exp(-a_0 u)\left[\frac{-2\sqrt{Sc}\exp(-u(\gamma-a_0))}{\sqrt{\pi u}} - 2\sqrt{Sc(\gamma-a_0)}\ \text{erf}\left(\sqrt{u\,(\gamma-a_0)}\right)\right]du.$$

2.4. NUSSELT NUMBER

The rate of heat transfer coefficient for the present problem is given as

$$Nu = \frac{\sqrt[3]{\nu^2/A}\,q_w''}{k(T_w^*-T_\infty^*)} = \frac{1}{\theta(0,t)} = \frac{\sqrt{F^*\,Q_H}}{1-\text{erfc}\left(\sqrt{Q_H\,t}\right)}\,. \tag{29}$$

2.5. SHERWOOD NUMBER

The rate of mass transfer coefficient is given by

$$Sh = \frac{\sqrt[3]{\nu^2/A}}{C_w^*-C_\infty^*}\frac{\partial C^*}{\partial y^*}\Big|_{y^*=0} = \frac{\partial \phi}{\partial y}\Big|_{y=0} = \delta_1+\delta_2-\delta_3, \tag{30}$$

where $\delta_\ell = \dfrac{\partial J_\ell}{\partial y}\Big|_{y=0}$ with $\ell = 1,2,3$ and

$$\delta_1 = \frac{1}{2}\Big[\frac{-2\sqrt{Sc}\exp(-\gamma t)}{\sqrt{\pi t}} - 2\sqrt{Sc\gamma}\ \text{erf}\left(\sqrt{\gamma t}\right)\Big],$$

$$\delta_2 = \frac{S^*}{2}\int_0^t \exp(H_1^* u)\left[\sqrt{Q_H}\ \text{erf}\left(\sqrt{Q_H(t-u)}\right) + \frac{\exp(-Q_H(t-u))}{\sqrt{\pi(t-u)}}\right]\left[\frac{-2\sqrt{Sc}\exp(-u(H_1^*+\gamma))}{\sqrt{\pi u}} - 2\sqrt{Sc(H_1^*+\gamma)}\ \text{erf}\left(\sqrt{u(H_1^*+\gamma)}\right)\right]du,$$

$$\delta_3 = \frac{S^*}{2}\int_0^t \exp(H_1^* u)\left[\sqrt{Q_H}\ \text{erf}\left(\sqrt{Q_H(t-u)}\right) + \frac{\exp(-Q_H(t-u))}{\sqrt{\pi(t-u)}}\right]\left[\frac{-2\sqrt{F^*}\exp(-u(H_1^*+Q_H))}{\sqrt{\pi u}} - 2\sqrt{F^*\left(H_1^*+Q_H\right)}\ \text{erf}\left(\sqrt{u\left(H_1^*+Q_H\right)}\right)\right]du.$$

3. Results and Discussions

We have formulated and solved the problem of the combined effects of heat and mass transfer with free convection MHD flow of an incompressible viscous fluid through a porous medium with constant heat flux at the plate. Final results are computed for a variety of physical parameters, which are presented by means of graphs. The results are obtained to illustrate the effects of magnetic field parameter M, dimensionless permeability parameter K, Grashof numbers for heat and mass transfer Gr and Gm, respectively, chemical reaction parameter γ, Prandtl number Pr, heat absorption parameter Q_H, radiation parameter R, Schmidt number Sc, Soret number Sr and dimensionless time t on the velocity, temperature and concentration profiles, as well as the skin friction coefficient, Nusselt number and Sherwood number.

Control of boundary layer flow is of practical significance. Several methods have been developed for the purpose of artificially controlling the behaviour of the boundary layer. The application of magnetohydrodynamic (MHD) principle is another method for affecting the flow field in the desired direction by altering the structure of the boundary layer. Figure 2 shows the velocity profiles for various values of magnetic parameter ($M = 0, 1, 2, 3$). The velocity curves show that the rate of transport is remarkably reduced with the increase of M. This result agrees qualitatively with the expectations, since the magnetic field exerts a retarding effect on the free convective flow.

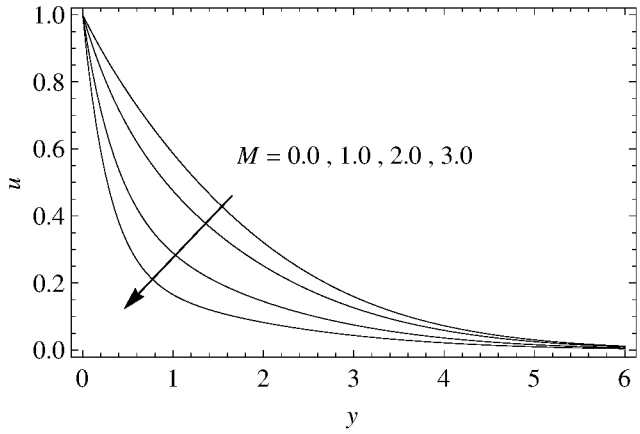

Fig. 2. Velocity profiles for different values of M when $t = 1$, $R = 0.5$, $Pr = 0.71$,$Gr = 1$, $K = 0.5$,$Gm = 1$, $\gamma = 0.5$, $Sc = 0.22$, $Sr = 2$, $Q_H = 0.1$.

The variation of velocity profile with dimensionless permeability parameter K is presented in Fig. 3. This figure clearly indicates that the value of velocity profile increases with increasing the dimensionless permeability parameter K. Physically, this result can be achieved when the holes of the porous medium are very large so that the resistance of the medium may be neglected.

Figure 4 is plotted to show the effect of Grashof number for heat transfer Gr on the velocity profiles. It is observed that an increase in Grashof number Gr leads to an increase in the velocity. This is due to the fact that buoyancy force enhances fluid

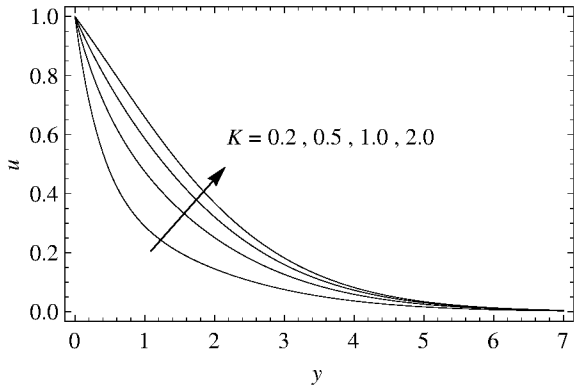

Fig. 3. Velocity profiles for different values of K when $M = 1$, $t = 1$, $R = 0.5$, $Pr = 0.71$, $Gr = 1$, $Gm = 1$, $\gamma = 0.5$, $Sc = 0.22$, $Sr = 2$, $Q_H = 0.1$.

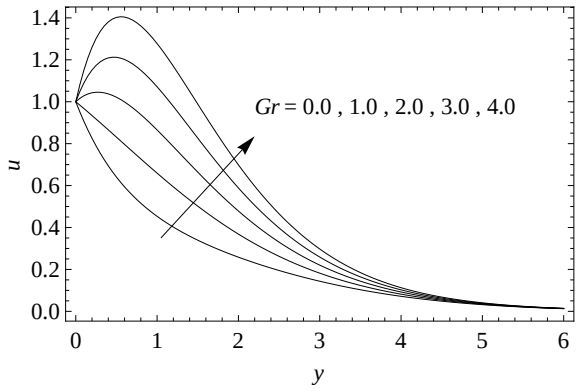

Fig. 4. Velocity profiles for different values of Gr when $M = 1$, $t = 1$, $R = 0.5$, $Pr = 0.71$, $K = 2$, $Gm = 1$, $\gamma = 0.5$, $Sc = 0.22$, $Sr = 2$, $Q_H = 0.1$.

velocity and increases the boundary layer thickness with increase in the values of Gr. It is also observed that distinctive peaks in the velocity profile occur in the fluid adjacent to the wall for higher values of Gr. The presence of the peaks indicates that the maximum value of fluid velocity occurs in the body of the fluid close to the surface and not at the surface. Figure 5 illustrates the effect of Grashof number for mass transfer Gm on the velocity profiles. As seen from this figure, the effect of Gm on the fluid velocity is the same as that of Gr. This fact is achieved by comparing Figs. 4 and 5.

Figure 6 represents the dimensionless velocity profiles u for increasing values of the chemical reaction parameter γ. It is seen from this figure that augmenting values

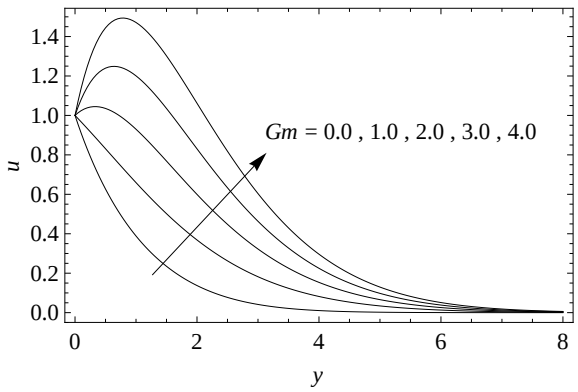

Fig. 5. Velocity profiles for different values of Gm when $M = 1$, $t = 1$, $R = 0.5$, $Pr = 0.71$, $Gr = 1$, $K = 2$, $\gamma = 0.5$, $Sc = 0.22$, $Sr = 2$, $Q_H = 0.1$.

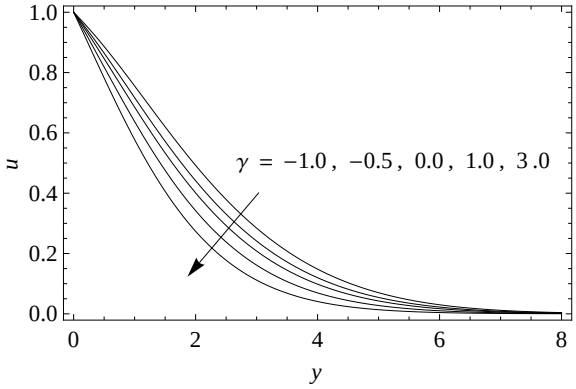

Fig. 6. Velocity profiles for different values of γ when $M = 1$, $t = 1$, $R = 0.5$, $Pr = 0.71$, $Gr = 1$, $K = 2$, $Gm = 1$, $Sc = 0.22$, $Sr = 2$, $Q_H = 0.1$.

of γ lead to fall in the velocity of the fluid. Figure 7 is sketched to show the effects of Prandtl number Pr on velocity profiles. Four different realistic values of $Pr = 0.71, 1, 7$ and 100 that are physically correspond to air, electrolytic solution, water, and engine oil, respectively are chosen. It is observed that the velocity decreases with increasing values of Prandtl number Pr. This is due to the fact that fluid with large Pr has high viscosity and small thermal conductivity, which make the fluid thick and causes a decrease in fluid velocity.

The influence of presence of the heat absorption parameter Q_H on the velocity distribution in the boundary layer is presented in Fig. 8. It is obvious that increasing

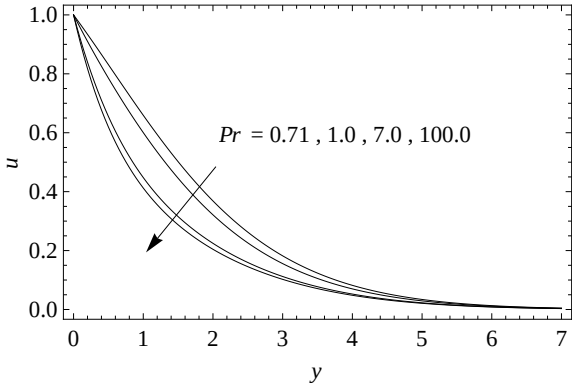

Fig. 7. Velocity profiles for different values of Pr when $M = 1$, $t = 1$, $R = 0.5$, $Gr = 1$, $K = 2$, $Gm = 1$, $\gamma = 0.5$, $Sc = 0.22$, $Sr = 2$, $Q_H = 0.1$.

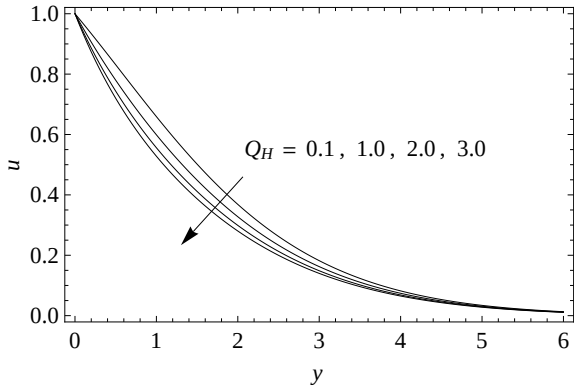

Fig. 8. Velocity profiles for different values of Q_H when $M = 1$, $t = 1$, $R = 0.5$, $Pr = 0.71$, $Gr = 1$, $K = 2$, $Gm = 1$, $\gamma = 0.5$, $Sc = 0.22$, $Sr = 2$.

the values of Q_H produces a decrease in the velocity distributions of the fluid. This is expected since the presence of a heat sink in the boundary layer absorbs energy, which in turn causes the temperature of the fluid to decrease. This decrease in temperature produces a decrease in the flow field due to the buoyancy effect, which couples the flow and thermal fields.

Figure 9 presents the effects of radiation parameter R on the velocity profiles. It is found that the velocity increases with increasing R. This result happens due to the fact that the large R values correspond to an increased dominance of conduction over radiation thereby increasing buoyancy force (thus, vertical velocity) and thickness of momentum boundary layer.

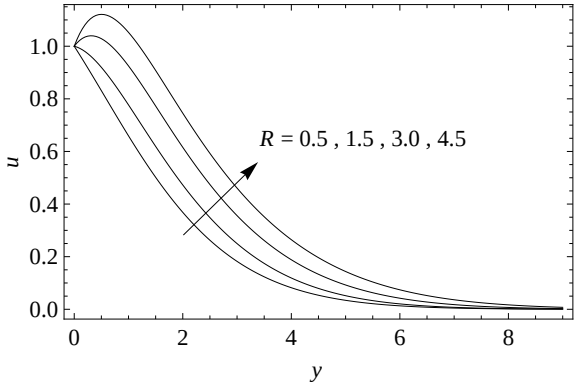

Fig. 9. Velocity profiles for different values of R when $M = 1$, $t = 1$, $Pr = 0.71$, $Gr = 1$, $K = 2$, $Gm = 1$, $\gamma = 0.5$, $Sc = 0.22$, $Sr = 2$, $Q_H = 0.1$.

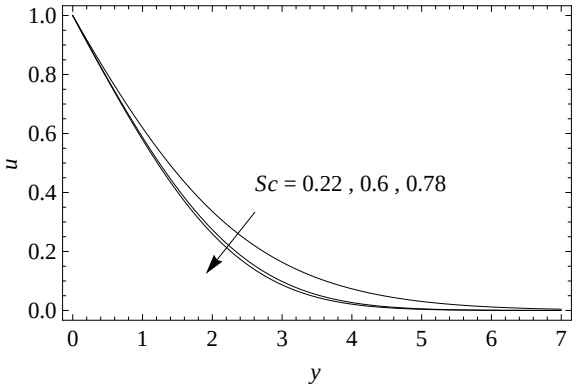

Fig. 10. Velocity profiles for different values of Sc when $M = 1$, $t = 1$, $R = 0.2$, $Pr = 0.71$, $Gr = 1$, $K = 2$, $Gm = 1$, $\gamma = 0.5$, $Sr = 2$, $Q_H = 0.1$.

Figure 10 shows the effect of Schmidt number Sc on the velocity profiles for $Sc = 0.22$ (hydrogen), 0.6 (water vapor), and 0.78 (ammonia). It is observed that the velocity decreases with increasing Schmidt number values due to the decrease in the molecular diffusivity, which results in a decrease in the concentration and velocity boundary layer thickness. On the other hand, the effect of Soret number Sr on the velocity profiles is completely opposite to that of Schmidt number Sc as clearly observed in Fig. 11. The variation of velocity profiles for different values of dimensionless time t is shown in Fig. 12. It is noticed that the velocity increases with the progression of time t. Moreover, the velocity in this figure takes the values of time t at the plate $(y = 0)$ and tends to zero for large values of y, which is a clear verification of the boundary conditions on the velocity given in (12).

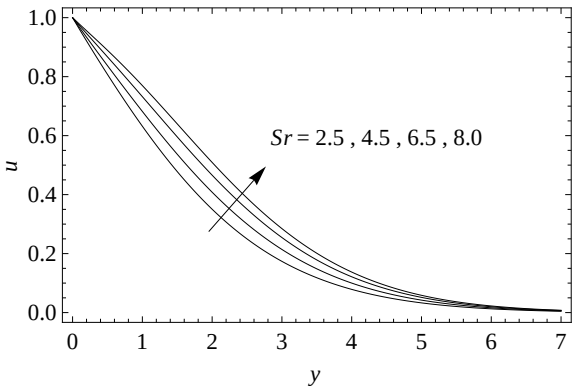

Fig. 11. Velocity profiles for different values of Sr when $M = 1$, $t = 1$, $R = 0.2$,$Pr = 0.71$, $Gr = 1$, $K = 2$, $Gm = 1$, $\gamma = 0.5$, $Sc = 0.22$, $Q_H = 0.1$.

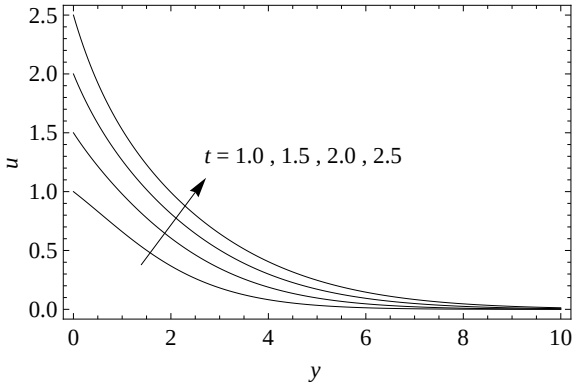

Fig. 12. Velocity profiles for different values of t when $M = 1$, $R = 0.5$, $Pr = 0.71$, $Gr = 1$, $K = 2$, $Gm = 1$, $\gamma = 0.5$, $Sc = 0.22$, $Sr = 2$, $Q_H = 0.1$.

It is observed in Fig. 13 that the fluid temperature θ is enhanced in the boundary layer with an increase in the thermal boundary layer thickness as the time t increases.

Figure 14 has been plotted to depict the variation of temperature profiles against y for different values of heat absorption parameter Q_H by fixing other physical parameters. It is observed from this graph that temperature θ decreases with increasing Q_H for the same reason mentioned above.

It is observed in Fig. 15 that the temperature θ increases as the radiation parameter R increases. This is because the large R values correspond to an increased dominance of conduction over radiation thereby increasing the thickness of the thermal boundary layer.

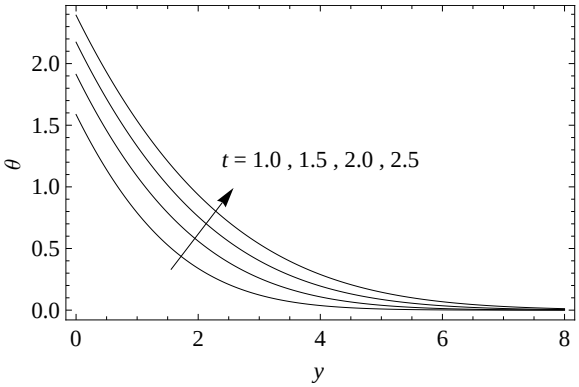

Fig. 13. Temperature profiles for different values of t when $Pr = 0.71$, $Q_H = 0.1$, $R = 0.5$.

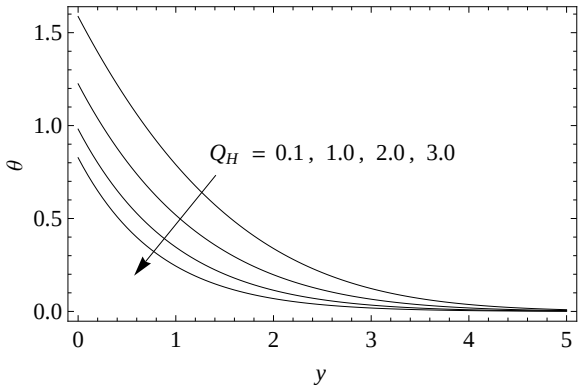

Fig. 14. Temperature profiles for different values of Q_H when $Pr = 0.71$, $R = 0.5$, $t = 1$.

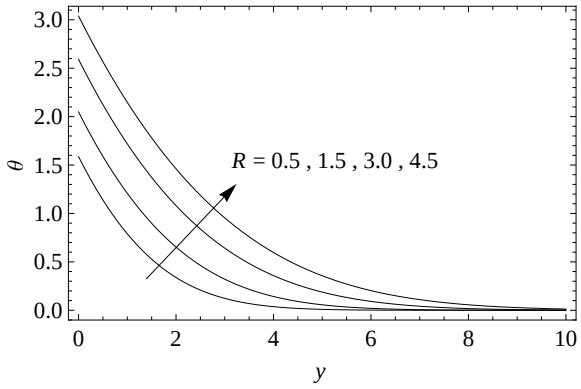

Fig. 15. Temperature profiles for different values of R when $Pr = 0.71$, $Q_H = 0.1$, $t = 1$.

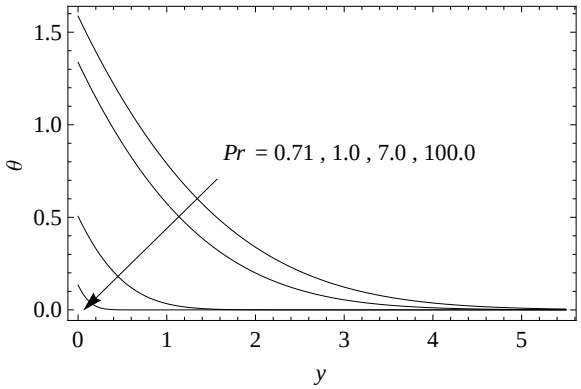

Fig. 16. Temperature profiles for different values of Pr when $Q_H = 3$, $R = 0.5$, $t = 1$.

It is evident from Fig. 16, that as the values of Pr increases from 0.71 to 100, we can find a decrease in the temperature profile and hence there is a decrease in thermal boundary layer thickness and more uniform temperature distribution across the boundary layer. Physically, this behaviour is due to the fact that with increasing Prandtl number, the thermal conductivity of the fluid decreases and the fluid viscosity increases which in turn results in a decrease in the thermal boundary layer thickness.

The evolution of concentration ϕ with progression of dimensionless time t is depicted in Fig. 17. It is clear that the concentration profiles increase with increasing t. Further, this figure verifies the boundary conditions of concentration given in (12). Initially, concentration takes the value 1 and later for large values of y ($y > 0$) it tends to zero with the increase of t.

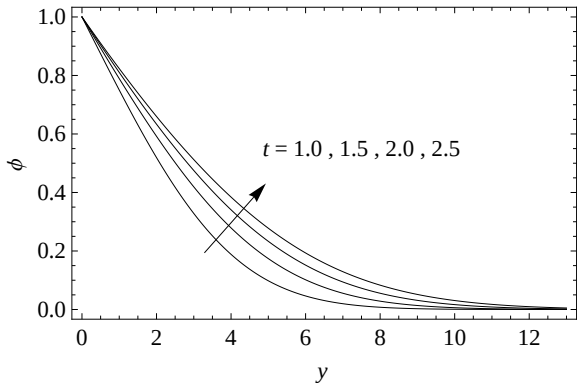

Fig. 17. Concentration profiles for different values of t when $Pr = 0.71$, $Sc = 0.22$, $\gamma = 0.2$, $Q_H = 0.1$, $Sr = 0.5$, $R = 0.5$.

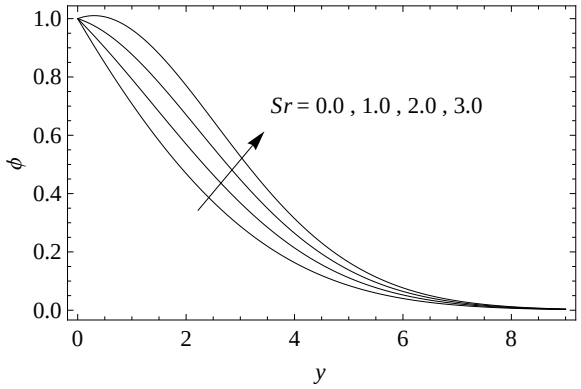

Fig. 18. Concentration profiles for different values of Sr when $Pr = 0.71$, $Sc = 0.22$, $\gamma = 0.2$, $Q_H = 0.1$, $R = 0.5$, $t = 1$.

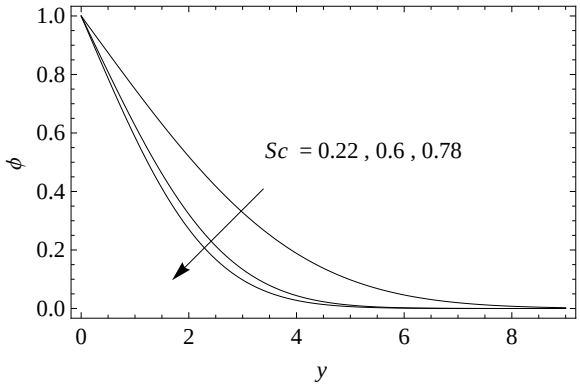

Fig. 19. Concentration profiles for different values of Sc when $Pr = 0.71$, $\gamma = 0.2$, $Q_H = 0.1$, $Sr = 0.5$, $R = 0.5$, $t = 1$.

The effects of Soret number Sr on the concentration profiles are shown in Fig. 18. The trend shows that ϕ increases with increasing values of Sr. Figure 19 observes the influence of Sc on the concentration ϕ. It is evident from this figure that the increasing values of Sc lead to fall in the concentration profiles. Physically, the increase of Sc means a decrease of molecular diffusion D. Hence, the concentration of the species is higher for small values of Sc and lower for large values of Sc.

The effect of the chemical reaction parameter γ on the concentration ϕ is shown in Fig. 20. It is noticed from this figure that there is a marked effect of increasing values of γ on concentration distribution in the boundary layer. It is clearly observed from this figure that increasing values of γ decreases the concentration of species in the

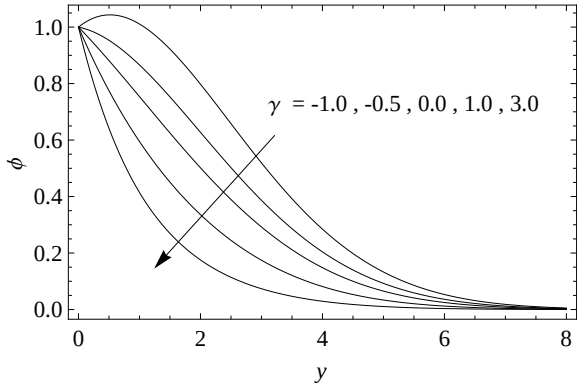

Fig. 20. Concentration profiles for different values of γ when $Pr = 0.714$, $Sc = 0.22$, $Q_H = 0.1$, $Sr = 0.5$, $R = 0.5$, $t = 1$.

boundary layer. This happens because large values of γ reduce the solutal boundary layer thickness and increase the mass transfer.

Variations of skin friction coefficient τ versus the dimensionless time t are plotted in Fig. 21 for various values of Prandtl number Pr and Grashof number of heat transfer Gr. It is revealed from this figure that τ greatly increases as t increases for all values of Pr and Gr. Also, it is noticed from this figure that with increasing values of Pr and for all values of t, τ slowly decreases when $Gr = 0$ while the opposite behaviour happens during $Gr > 0$. Moreover, τ is decreased on increasing Gr for all values of t and Pr. Figure 21 also shows that the influence of Gr on τ for fluids having small Pr is more pronounced than those having large Pr. Furthermore, the effect of Pr on τ is found to be more significant with large values of Gr ($Gr = 2$) than small values of Gr ($Gr = 0$).

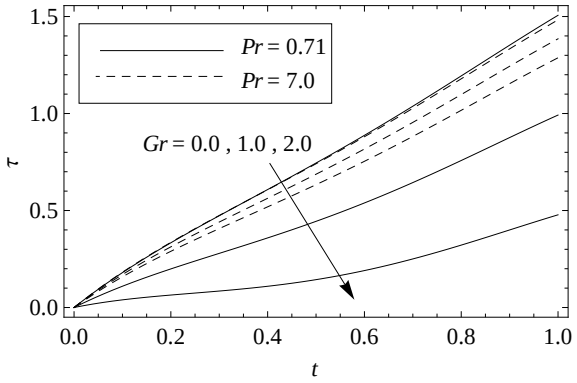

Fig. 21. Skin friction variation for various values of Gr, Pr and t when $M = 1$, $K = 0.5$, $R = 0.2$, $Gm = 1$, $\gamma = 0.5$, $Sc = 2$, $Sr = 2.5$, $Q_H = 0.1$.

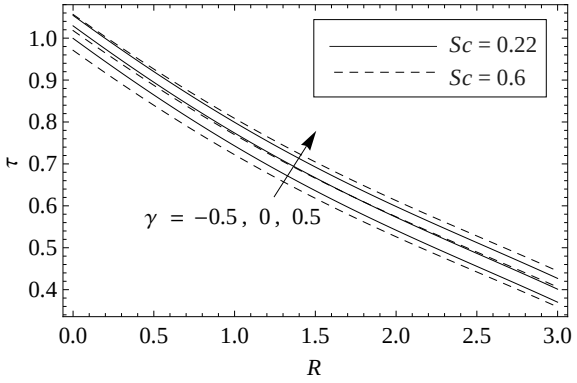

Fig. 22. Skin friction variation for various values of Sc, γ and R when $M = 1$, $K = 0.5$, $Gm = 1$, $Sr = 2.5$, $Pr = 0.71$, $Gr = 1$, $Q_H = 0.1$, $t = 1$.

It is noticed from Fig. 22 that the skin friction τ is greatly decreased as the radiation parameter R increased for all values of γ and Sc. Also, Fig. 22 illustrates that, for given R and Sc, τ is increased with an increase of chemical reaction parameter γ. Furthermore, for a given R and increasing values of Sc, τ is decreased in case of generative reaction $\gamma < 0$ while the reverse behaviour is happened in case of destructive reaction $\gamma > 0$. Moreover, in case of $\gamma = 0$, τ reduces slightly when $R \leq R_0 \simeq 1.6$ and then rises slowly when $R > R_0$.

Figure 23 shows the variation of τ versus the magnetic field parameter M for different values of heat absorption parameter Q_H and dimensionless permeability parameter K. It is clear from this figure that for all values of M, τ is decreased with an increase of K for all values of Q_H. A quite opposite attitude is shown on τ

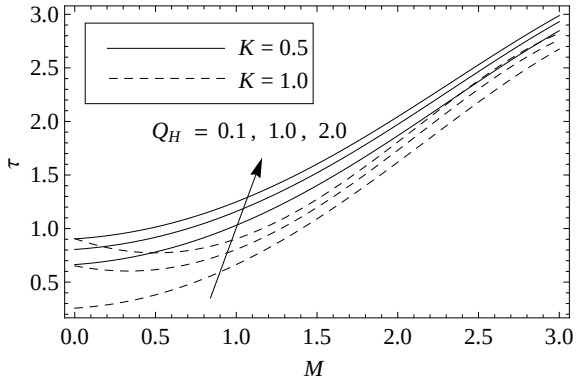

Fig. 23. Skin friction variation for various values of Q_H, K and M when $Gm = 1$, $Sr = 2.5$, $Pr = 0.71$, $Gr = 1$, $t = 1$, $Sc = 0.5$, $\gamma = 1$, $R = 0.2$.

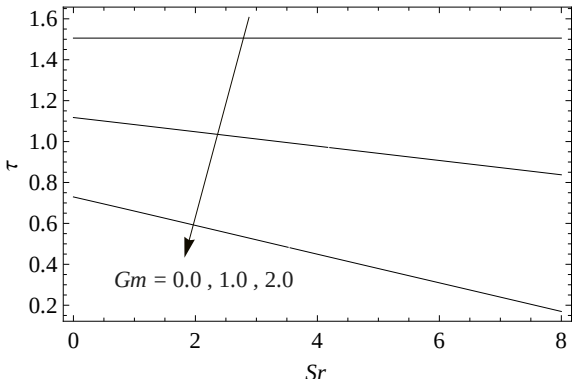

Fig. 24. Skin friction variation for various values of Gm and Sr when $Pr = 0.71$, $Gr = 1$, $Sc = 0.5$, $\gamma = 1$, $R = 0.2$, $K = 0.5$, $Q_H = 0.1$, $t = 1$, $M = 1$.

with increasing values of Q_H for given M and K. Furthermore, and for all values of Q_H, τ is induced as M increases during $K = 0.5$. As K increases to 1, and when $Q_H > 0.1$, τ is slightly decreased when $M \leq M_0 \simeq 0.4$ whereas the reverse effect is noticed when $M > M_0$. Moreover, the maximum effect of Q_H on τ is attained in the hydrodynamic flow case ($M = 0$), when the magnetic field is absent. Figure 24 illustrates that, for given values of Soret number Sr, τ is decreased with an increase in the values of Grashof number for mass transfer Gm. Also, an increase in the values of Sr leads to a decrease in the values of τ for $Gm > 0$. In contrast, no effect is noticed on τ when $Gm = 0$ for any value of Sr.

From Fig. 25 it is noticed that the Sherwood number decreases as the radiation parameter R is increased for all values of Sr and t, while it increases with increasing values of Sr and t for any value of R. Figure 26 is aimed to explore the effects of

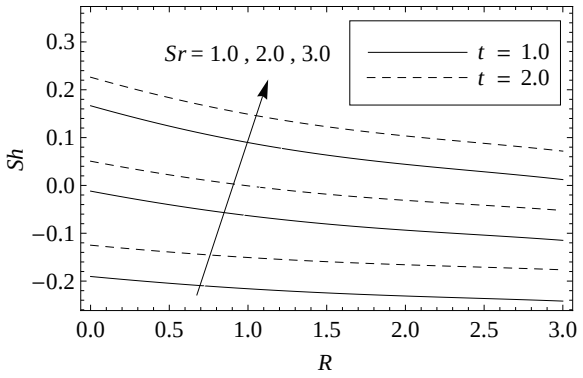

Fig. 25. Sherwood number variation for various values of Sr, t and R when $Sc = 0.3$, $\gamma = 0.2$, $Pr = 0.71$, $Q_H = 0.1$.

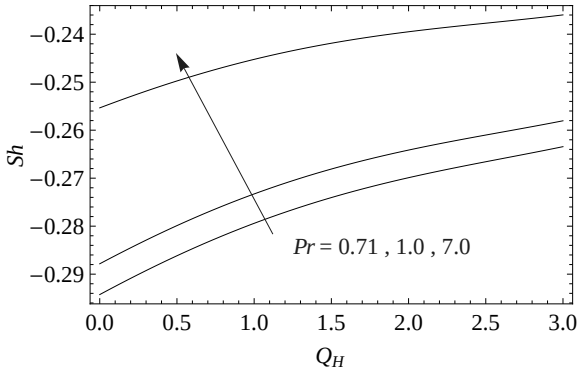

Fig. 26. Sherwood number variation for various values of Pr and Q_H when $\gamma = 0.2$, $Sc = 0.3$, $Sr = 0.5$, $t = 1$, $R = 1$.

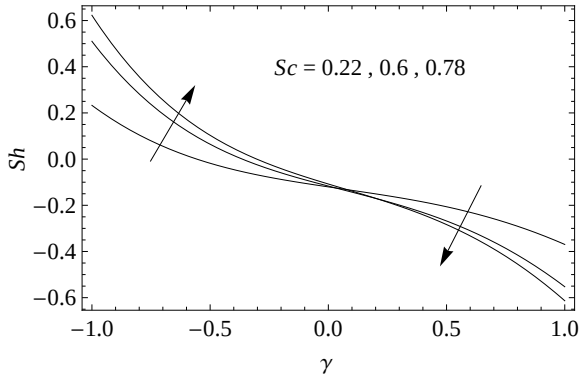

Fig. 27. Sherwood number variation for various values of Sc and γ when $Pr = 0.71$, $t = 1$, $Q_H = 1$, $R = 1$, $Sr = 1$.

Prandtl number Pr on the Sherwood number Sh versus heat absorption parameter Q_H. It is noticed that Sh is increased as Q_H increases for all values of Pr. The same attitude happens with increasing values of Pr for any selected value of Q_H.

It can be seen from Fig. 27 that the Sherwood number Sh is reduced with an increase of γ for all values of Schmidt number Sc. Also, this figure illustrates that with increasing values of Sc, Sh is increasing when $\gamma \leq \gamma_0 \simeq 0.1$ and it is decreasing when $\gamma > \gamma_0$.

The effects of Q_H and t on the Nusselt number Nu versus the radiation parameter R are shown in Fig. 28. It is clear that Nu is greatly decreased with increasing R. Also, for all values of R, higher Nusselt numbers are noticed at large values of Q_H. Moreover, an increase in the values of t leads to a decrease in the values of Nusselt number for all values of Q_H and R. Further, the maximum effect of t on Nu

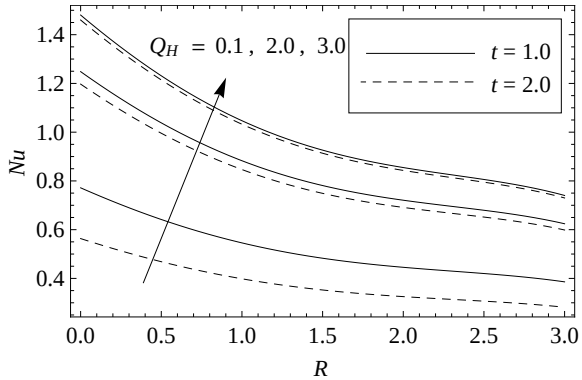

Fig. 28. Nusselt number variation for various values of Q_H, t and R when $Pr = 0.71$.

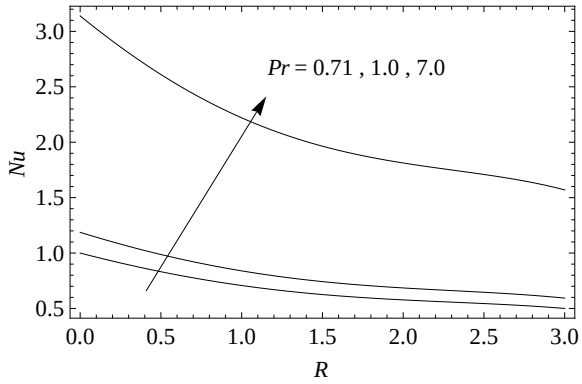

Fig. 29. Nusselt number variation for various values of Pr and R when $Q_H = 1$, $t = 1$.

occurs for lower values of Q_H ($Q_H = 0.1$) whereas the effect of Q_H becomes more significant for higher values of t ($t = 2$).

Finally, Fig. 29 reveals, for a given Pr, that the effect of increasing values of R is to reduce Nusselt number Nu. A contrast influence is noticed on Nu with increasing values of Pr for a selected value of R.

4. CONCLUSIONS

The problem of unsteady MHD free convection flow of an incompressible and electrically conducting fluid past a vertical plate embedded in a porous medium with constant heat flux is provided. The exact solutions are obtained by using Laplace transform method. The significant findings are summarized below:

(1) The impact of permeability parameter K, Grashof numbers for heat transfer Gr and mass transfer Gm, chemical reaction parameter γ, heat absorption parameter Q_H and radiation parameter R on the skin friction shows quite the opposite effect to that of the velocity of the fluid.

(2) Similar to the first conclusion, the influence of Pr, Q_H, R and t on Nusselt number Nu is quite the reverse to that of the temperature of the fluid.

(3) The fluid concentration decreases with increasing values of γ and Sc, whereas it increases when Sr and t are increased.

(4) Sherwood number profiles show an increase with augmenting Pr, Sr and t while the reverse attitude happens with increasing γ and R.

ACKNOWLEDGEMENT

The authors are very thankful to the reviewers for their encouraging comments and constructive suggestions to improve the presentation of the manuscript. Also, the authors would like to express their gratitude to King Khalid University, Saudi Arabia, for providing administrative and technical support.

REFERENCES

[1] MUTHUCUMARASWAMY, R., P. GANESAN, V. M. SOUNDALGEKAR. Heat and Mass Transfer Effects on Flow Past an Impulsively Started Vertical Plate. *Acta Mechanica*, **146** (2001), No. **1-2**, 1-8.

[2] CHAUDHARY, R. C., A. JAIN. Combined Heat and Mass Transfer Effects on MHD Free Convection Flow Past an Oscillating Plate embedded in Porous Medium. *Rom. J. Phys*, **52** (2007), No. **5-7**, 505-524.

[3] SIVAIAH, M., A. S. NAGARAJAN, P. S. REDDY. Heat and Mass Transfer Effects on MHD Free Convective Flow Past a Vertical Porous Plate. *The ICFAI University Journal of Computational Mathematics*, **2** (2009), No. **2**, 14-21.

[4] DAS, K., S. JANA. Heat and Mass Transfer Effects on Unsteady MHD Free Convection Flow Near a Moving Vertical Plate in Porous Medium. *Bull. Soc. Math. Banja Luka*, **17** (2010), No. **10**, 15-32.

[5] DONALD, A. N., A. BEJAN. Convection in Porous Media, Springer Science & Business Media, 2006.

[6] CHAMKHA, A. J. Thermal Radiation and Buoyancy Effects on Hydromagnetic Flow over an Accelerating Permeable Surface with Heat Source or Sink. *International Journal of Engineering Science*, **38** (2000), No. **15**, 1699-1712.

[7] CHAMKHA, A. J. Unsteady MHD Convective Heat and Mass Transfer past a Semi-infinite Vertical Permeable Moving Plate with Heat Absorption. *International Journal of Engineering Science*, **42** (2004), No. **2**, 217-230.

[8] KIM, Y. J. Unsteady MHD Convection Flow of Polar Fluids past a Vertical Moving Porous Plate in a Porous Medium. *International Journal of Heat and Mass Transfer*, **44** (2001), No. **15**, 2791-2799.

[9] RAHMAN, M. M., M. A. SATTAR. Magnetohydrodynamic Convective Flow of a Micropolar Fluid past a Continuously Moving Vertical Porous Plate in the Presence of Heat Generation/absorption. *Journal of Heat Transfer*, **128** (2006), No. **2**, 142-152.

[10] HAYAT, T., Z. ABBAS. Heat Transfer Analysis on the MHD Flow of a Second Grade Fluid in a Channel with Porous Medium. *Chaos, Solitons & Fractals*, **38** (2008), No. **2**, 556-567.

[11] RAJESH, V., S. V. K. VARMA. Radiation Effects on MHD Flow through a Porous Medium with Variable Temperature or Variable Mass Diffusion. *Int. J. of Appl. Math and Mech*, **6** (2010), No. **1**, 39-57.

[12] SATTAR, M. A. Free Convection and Mass Transfer Flow through a Porous Medium past an Infinite Vertical Porous Plate with Time Dependent Temperature and Concentration. *Ind. J. Pure Appl. Math*, **23** (1994), 759-766.

[13] REES, D. A. S., I. POP. Free Convection induced by a Vertical Wavy Surface with Uniform Heat Flux in a Porous Medium. *Journal of Heat Transfer*, **117** (1995), No. **2**, 547-550.

[14] ACHARYA, M., G. C. DASH, L. P. SINGH. Magnetic Field Effects on the Free Convection and Mass Transfer Flow through Porous Medium with Constant Suction and Constant Heat Flux. *Indian Journal of Pure and Applied Mathematics*, **31** (2000), No. **1**, 1-18.

[15] CHENG, C. Y. Natural Convection Heat and Mass Transfer Near a Vertical Wavy Surface with Constant Wall Temperature and Concentration in a Porous Medium. *International Communications in Heat and Mass Transfer*, **27** (2000), No. **8**, 1143-1154.

[16] TOKI, C. J. Free Convection and Mass Transfer Flow Near a Moving Vertical Porous Plate: an Analytical Solution. *Journal of Applied Mechanics*, **75** (2008), No. **1**, 11014 (8 pages).

[17] RAJESH, V., S. V. K. VARMA. Heat Source Effects on MHD Flow past an Exponentially Accelerated Vertical Plate with Variable Temperature through a Porous Medium. *Int. J. of Appl. Math and Mech*, **6** (2010), No. **12**, 68-78.

[18] CHAUDHARY, R. C., A. JAIN. An Exact Solution of Magnetohydrodynamic Convection Flow past an Accelerated Surface embedded in a Porous Medium. *International Journal of Heat and Mass Transfer*, **53** (2010), No. **7**, 1609-1611.

[19] DAS, K. Exact Solution of MHD Free Convection Flow and Mass Transfer Near a moving Vertical Plate in Presence of Thermal Radiation. *African J. Math. Phys*, **8** (2010), 29-41.

[20] PAL, D., B. TALUKDAR. Buoyancy and Chemical Reaction Effects on MHD mixed Convection Heat and Mass Transfer in a Porous Medium with Thermal Radiation and Ohmic Heating. *Communications in Nonlinear Science and Numerical Simulation*, **15** (2010), No. **10**, 2878-2893.

[21] SETH, G. S., M. S. ANSARI, R. NANDKEOLYAR. MHD Natural Convection Flow with Radiative Heat Transfer past an Impulsively Moving Plate with Ramped Wall Temperature. *Heat and Mass Transfer*, **47** (2011), No. **5**, 551-561.

[22] KHAN, I., F. ALI, S. SHAFIE, N. MUSTAPHA. Effects of Hall Current and Mass Transfer on the Unsteady Magnetohydrodynamic Flow in a Porous Channel. *Journal of the Physical Society of Japan*, **80** (2011), No. **6**, 064401 (6 pages).

[23] SEDDEEK, M. A., A. A. DARWISH, M. S. ABDELMEGUID. Effects of Chemical Reaction and Variable Viscosity on Hydromagnetic Mixed Convection Heat and Mass Transfer for Hiemenz Flow through Porous Media with Radiation. *Communications in Nonlinear Science and Numerical Simulation*, **12** (2007), No. **2**, 195-213.

[24] MAHDY, A. Effect of Chemical Reaction and Heat Generation or Absorption on Double-diffusive Convection from a Vertical Truncated Cone in Porous Media with

Variable Viscosity. *International Communications in Heat and Mass Transfer*, **37** (2010), No. **5**, 548-554.

[25] ALHARBI, S. M., M. A. A. BAZID, M. S. EL GENDY. Heat and Mass Transfer in MHD Visco-elastic Fluid Flow through a Porous Medium over a Stretching Sheet with Chemical Reaction. *Applied Mathematics*, **1** (2010), No. **06**, 446.

[26] SHATEYI, S., S. MOTSA. Unsteady Magnetohydrodynamic Convective Heat and Mass Transfer Past an Inginite Vertical Plate in a Porous Medium with Thermal Radiation, Heat Generation/Absorption and Chemical Reaction, pages 145-162. INTECH Open Access Publisher, 2011.

[27] KASIM, A. R. M., N. F. MOHAMMAD, S. SHAFIE. Unsteady MHD Mixed Convection Flow with Heat and Mass Transfer over a Vertical Plate in a Micropolar Fluid-saturated Porous Medium. *Journal of Applied Science and Engineering*, **16** (2013), No. **2**, 141-150.

[28] ALI, F., I. KHAN, S. SHAFIE, N. MUSTHAPA. Heat and Mass Transfer with Free Convection MHD Flow past a Vertical Plate embedded in a Porous Medium. *Mathematical Problems in Engineering*, Vol. **2013**, Article ID 346281, 13 pages.